# Dark pulse quantum dot diode laser

**Mingming Feng,[1,2] Kevin L. Silverman,[3] Richard P. Mirin,[3] and Steven T. Cundiff[1,2,*]**

[1] *JILA, University of Colorado and National Institute of Standards and Technology, Boulder, CO 80309-0440, USA*
[2] *Department of Physics, University of Colorado, Boulder, CO 80309-0390 USA*
[3] *National Institute of Standards and Technology, Boulder, CO 80305 USA*
**cundiff@jila.colorado.edu*

**Abstract:** We describe an operating regime for passively mode-locked quantum dot diode laser where the output consists of a train of dark pulses, i.e., intensity dips on a continuous background. We show that a dark pulse train is a solution to the master equation for mode-locked lasers. Using simulations, we study stability of the dark pulses and show they are consistent with the experimental results.



**OCIS codes:** (140.2020) Diode Lasers; (190.5530) Pulse propagation and temporal solitons.

## References and links

1. A. M. Weiner, *Ultrafast Optics* (Wiley, 2009).
2. J.-C. Diels, and W. Rudolp, *Ultrashort Laser Pulse Phenomena* (Academic Press, 2006) 2nd ed.
3. S. Mukamel, *Principles of Nonlinear Optical Spectroscopy*, (Oxford University Press, 1995).
4. S. T. Cundiff, "Coherent spectroscopy of semiconductors," Opt. Express **16**(7), 4639–4664 (2008).
5. C. Dorrer, "High-speed measurements for optical telecommunication systems," IEEE J. Sel. Top. Quantum Electron. **12**(4), 843–858 (2006).
6. S. T. Cundiff, and J. Ye, "Colloquium: Femtosecond optical frequency combs," Rev. Mod. Phys. **75**(1), 325–342 (2003).
7. F. Krausz, and M. Ivanov, "Attosecond physics," Rev. Mod. Phys. **81**(1), 163–234 (2009).
8. Y. Kivshar, and B. Luther-Davies, "Dark optical solitons: physics and applications," Phys. Rep. **298**(2-3), 81–197 (1998).
9. M. Nakazawa, and K. Suzuki, "Generation of a pseudorandom dark soliton data train and its coherent detection by one-bit-shifting with a mach-zehnder interferometer," Electron. Lett. **31**(13), 1084–1085 (1995).
10. D. J. Richardson, R. P. Chamberlin, L. Dong, and D. N. Payne, "Experimental demonstration of 100ghz dark soliton generation and propagation using a dispersion decreasing fiber," Electron. Lett. **30**(16), 1326–1327 (1994).
11. O. G. Okhotnikov, and F. M. Araujo, "Pulse generation through optical switching in phase driven loop mirror," Electron. Lett. **31**(25), 2197–2198 (1995).
12. A. M. Weiner, J. P. Heritage, R. J. Hawkins, R. N. Thurston, E. M. Kirschner, D. E. Leaird, and W. J. Tomlinson, "Experimental observation of the fundamental dark soliton in optical fibers," Phys. Rev. Lett. **61**(21), 2445–2448 (1988).
13. M. Haelterman, and P. Emplit, "Optical dark soliton trains generated by passive spectral filtering technique," Electron. Lett. **29**(4), 356–357 (1993).
14. P. Emplit, M. Haelterman, R. Kashyap, and M. DeLathouwer, "Fiber Bragg grating for optical dark soliton generation," IEEE Photon. Technol. Lett. **9**(8), 1122–1124 (1997).
15. D. M. Pataca, M. L. Rocha, R. Kashyap, and K. Smith, "Bright and dark pulse generation in an optically modelocked fiber laser at 1.3 μm," Electron. Lett. **31**(1), 35–36 (1995).
16. M. Kauer, J. R. A. Cleaver, J. J. Baumberg, and A. P. Heberle, "Femtosecond dynamics in semiconductor lasers: Dark pulse formation," Appl. Phys. Lett. **72**(13), 1626–1628 (1998).
17. J. Zimmermann, S. T. Cundiff, G. von Plessen, J. Feldmann, M. Arzberger, G. Bohm, M. C. Amann, and G. Abstreiter, "Dark pulse formation in a quantum-dot laser," Appl. Phys. Lett. **79**(1), 18–20 (2001).
18. H. Zhang, D. Y. Tang, L. M. Zhao, and X. Wu, "Dark pulse emission of a fiber laser," Phys. Rev. A **80**(4), 045803 (2009).
19. H. A. Haus, "Theory of mode-locking with a fast saturable absorber," J. Appl. Phys. **46**(7), 3049–3058 (1975).
20. E. U. Rafailov, M. A. Cataluna, and W. Sibbett, "Mode-locked quantum-dot lasers," Nat. Photonics **1**(7), 395–401 (2007).
21. M. van der Poel, and J. M. Hvam, "Ultrafast dynamics of quantum-dot semiconductor optical amplifiers," J. Mater. Sci. Mater. Electron. **18**(S1), 51–55 (2007).
22. S. Tsuda, W. H. Knox, S. T. Cundiff, W. Y. Jan, and J. E. Cunningham, "Mode-locking ultrafast solid-state lasers with saturable Bragg reflectors," IEEE J. Sel. Top. Quantum Electron. **2**(3), 454–464 (1996).
23. A. E. Siegman, *Lasers* (University Science Books, 1986)
24. J.-C. Diels, and W. Rudolph, *Ultrashort Laser Pulse Phenomena*, 2nd edition, (Academic Press, 2006)
25. H. A. Haus, "Parameter ranges for CW passive mode-locking," IEEE J. Quantum Electron. **12**(3), 169–176 (1976).

#127499 - $15.00 USD Received 23 Apr 2010; revised 22 May 2010; accepted 25 May 2010; published 7 Jun 2010

26. F. X. Kärtner, J. A. D. Au, and U. Keller, "Mode-locking with slow and fast saturable absorbers - What's the difference?" IEEE J. Sel. Top. Quantum Electron. **4**(2), 159–168 (1998).
27. K. L. Silverman, R. P. Mirin, S. T. Cundiff, and A. G. Norman, "Direct measurement of polarization resolved transition dipole moment in InGaAs/GaAs quantum dots," Appl. Phys. Lett. **82**(25), 4552–4554 (2003).
28. T. Sylvestre, S. Coen, P. Emplit, and M. Haelterman, "Self-induced modulational instability laser revisited: normal dispersion and dark-pulse train generation," Opt. Lett. **27**(7), 482–484 (2002).

## 1. Introduction

Mode-locked lasers generate trains of ultrashort optical pulses over a wide range of durations, from tens of picoseconds down to a few femtoseconds and with repetition rates that range from a few megahertz to tens of gigahertz [1, 2]. Mode-locked lasers have traditionally been used in applications based on the time resolution provided by the ultrashort pulses they generate. Examples of such applications include the time-domain spectroscopy of molecules [3], semiconductors [4] or in high speed measurements for optical telecommunications [5]. However, the development of femtosecond comb techniques has expanded the use of mode-locked lasers into optical frequency metrology, enabled optical atomic clocks [6] and has been essential to the breakthrough to the attosecond regime [7].

In addition producing bright pulses, a mode-locked laser can produce dark pulses, although this operating regime is rare. A dark pulse is a brief decrease in intensity on a stable continuous wave. A close analogy to a dark pulse in a mode-locked laser is a dark optical soliton. Optical dark solitons are solutions to the nonlinear Schrödinger equation (NLSE) that have been the subject of much theoretical investigation [8]. The NLSE describes propagation in nonlinear media such as optical fiber, but it does not contain dissipative terms such as gain, loss and their saturation, which are present in a mode-locked laser. Optical dark solitons are predicted to have many properties of practical importance such as existence in the normal dispersion regime, lack of a threshold and resistance to Gordon-Haus jitter. Experimental work on dark solitons has been limited because they have been difficult to generate. Different techniques have been proposed and demonstrated to generate a single dark pulse or dark pulse train; most of them are based on external manipulation of laser light using pulse-shaping techniques. Methods include intensity modulation of a CW laser beam by an electro-optic modulator [9], nonlinear conversion of a beat frequency signal in a normal dispersion decreasing fiber [10], electro-optic phase modulation in a linear loop mirror [11], and passive filtering of a mode-locked bright pulse train with a spatial mask [12, 13], with a fiber Bragg grating [14], or with an active FM mode locking technique [15]. Also, dark pulse generation has previously been observed in semiconductor amplifiers after injection of a bright pulse [16,17], however the pulse train was not stable and eventually decays. Recently, the generation of dark pulses in a mode-locked fiber laser was reported when the cavity dispersion was normal and the non-linear polarization rotation was adjusted to give reverse saturable absorption [18].

Here, we demonstrate the generation of a dark pulse train using a passively mode-locked semiconductor quantum-dot diode laser. We show that a dark pulse is a straightforward solution to the linearized version of the equation that describes the operation of a passively mode-locked laser [19]. While having similarities to dark solitons, we do not believe that these pulses are dark solitons as they are not transform limited. To determine if the dark-pulse solution is stable, and over what range of parameters, we perform simulations for the full (not linearized) equation. We show that the parameters of our laser fall in the range predicted to have stable dark pulses.

## 2. Experiment

We demonstrate dark pulses using an external cavity semiconductor diode laser (Fig. 1). The gain section is a 5 mm long single-mode semiconductor ridge waveguide with InGaAs self-assembled quantum dots (QDs) buried in the core. QDs feature complex gain dynamics that provide the necessary flexibility to operate where dark pulses are stable [20, 21]. Light amplified by the quantum dot active region is collimated, filtered by a Fabry-Perot etalon and focused on a saturable absorber to initiate mode-locking. The saturable absorbing medium, a

#127499 - $15.00 USD Received 23 Apr 2010; revised 22 May 2010; accepted 25 May 2010; published 7 Jun 2010

few intentionally damaged semiconductor wells [22], was grown in an integrated resonant structure to increase the electric field intensity and lower the saturation fluence. The saturable absorber structure also acts as an end mirror for the laser cavity. Spectral filtering to tune and restrict the lasing bandwidth is provided by a Fabry-Perot etalon with a transmission bandwidth of 10 nm. The flat facet of the semiconductor diode is used as the output coupler with a reflectivity of approximately 35%. When the laser cavity is well aligned, lasing action occurs with 60 mA of current injected into the gain medium.

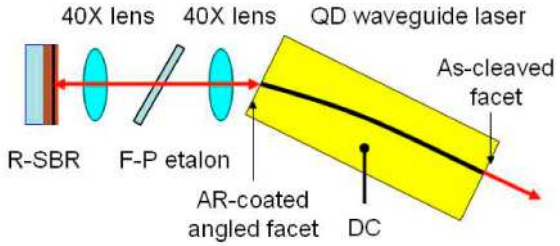


Fig. 1. Schematic of external cavity diode laser (R-SBR: resonant saturable Bragg reflector).

Subthreshold electroluminescence from the QD gain region is shown in Fig. 2(a). A fit to the spectrum at low current gives a ground state peak at 1169 nm and a full width at half maximum of 56 nm. As the injection level increases, clear state filling, typical of QDs, is observed as emission from an excited state becomes appreciable.

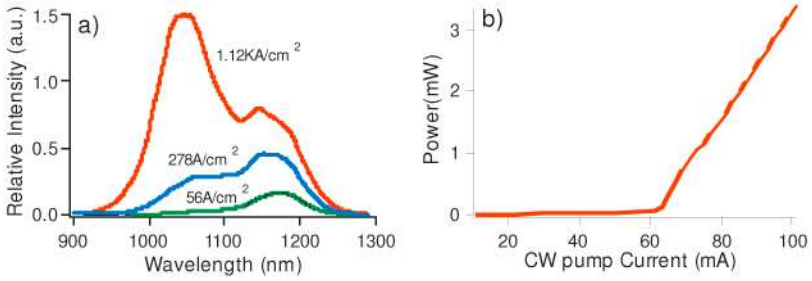


Fig. 2. Optical characteristics of the laser. (a) Electroluminescence from the QDs gain. (b) Light-current characteristics.

The threshold current for this device is approximately 60 mA after careful alignment of the external cavity. A representative optical power versus injected current trace is shown in Fig. 2(b). Output power saturation does not occur until the pump current is above 200 mA.

The resonant saturable Bragg reflector (R-SBR) was grown by molecular beam epitaxy (MBE) on a GaAs substrate. The saturable absorber in the SBR is an InGaAs:Be,Er doped multi-quantum well. To achieve high modulation depth and low saturation fluence, a resonant structure is used. The quantum well stack is positioned in the center of a GaAs cavity layer. The top and bottom mirrors were formed by an alternating stack of λ/4 AlAs and GaAs layers. The bottom mirror had 22.5 pairs and the top mirror had 2 pairs. The low intensity reflectance spectrum for this device is shown in Fig. 3(a). The resonant wavelength is 1168 nm and the bandwidth is 10 nm.

We characterized the saturation of the absorber by focusing a pulsed laser tightly on the surface of the R-SBR and measuring the reflectivity as a function of power. The pulse width of the laser was approximately 100 fs and the repetition rate was 82 MHz. The center wavelength matched the resonant condition of the R-SBR. Since the pulse width was much shorter than the recovery time of the InGaAs:Be,Er QWs, no appreciable relaxation occurs during the excitation process, and it is appropriate to report the reflectivity as a function of the integrated energy in the pulse. These data are shown in Fig. 3(b). A simple fit to this curve using a standard model for saturation [23] yields the saturation fluence, $F$, of 4 μJ/cm$^2$ (focused spot area is about 8 μm$^2$). Figure 3(b) also shows that even at very high fluence the

#127499 - $15.00 USD Received 23 Apr 2010; revised 22 May 2010; accepted 25 May 2010; published 7 Jun 2010

reflectivity does not recover to 100%. This nonsaturable loss is due to defects in the QW material or scattering loss from the layers of the resonant structure.

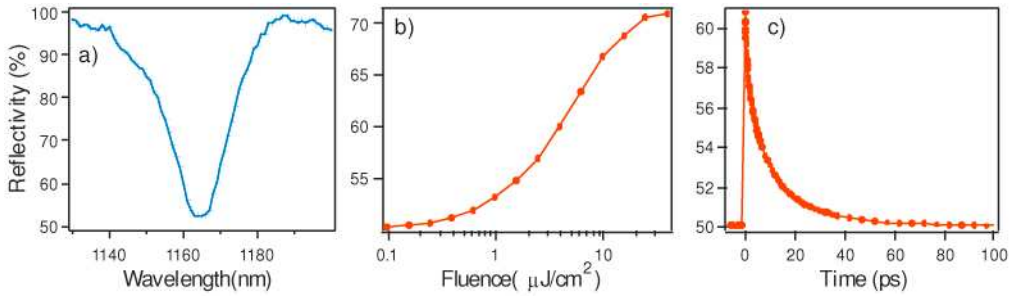


Fig. 3. Characterization of the saturable Bragg reflector. (a) Low intensity reflection spectrum, (b) reflectivity vs. fluence., (c) temporal response, the black curve is a 10 ps single exponential decay fit to the measured data.

We characterized the temporal response of the absorber with a standard time-resolved pump-probe technique [24]. We employed 100 fs pulses resonant with the cavity of the R-SBR. The temporal response is shown in Fig. 3(c). A single exponential fit yields a time constant, $T_r$, of 10 ps. We used this time, along with the saturation data above, to estimate the saturation properties of the absorber under CW conditions. We balanced the rate of decay with the rate of absorption using $I_q = (F / T_r)A$. This leads to a CW absorber saturation power, $I_q$, of 8 mW if the spot size, $A$, is 2 μm$^2$.

We monitored the output of the laser using a fast photodetector and recorded the output on a high-speed oscilloscope (Fig. 4). A dark pulse train is clearly observed for currents above 110 mA.. The width of the pulses is measured to be 90 ps (a fit is shown in red in Fig. 4), and the modulation depth is approximately 70% (the ratio of the minimum power of the dark pulse to continuous wave (CW) level). We carefully calibrated the measurement system with a source of ultrafast bright pulses and determined the time resolution to be about 60 ps, mostly limited by the sampling oscilloscope. This calibration also confirms that the signal is due to dark pulses and not artifacts in the detection system. A simple deconvolution of the instrument response function yields a true pulse width of 70 ps. The excursion above the CW level preceding each dark pulse is due to ringing in the electronics, which is also evident when measuring bright pulses. Measurements using time-correlated single photon counting confirm that the train consists only of dark pulses. Based on the calibration, we conclude that the pulses are not “black” pulses, i.e., going to zero intensity, but rather “gray” pulses.

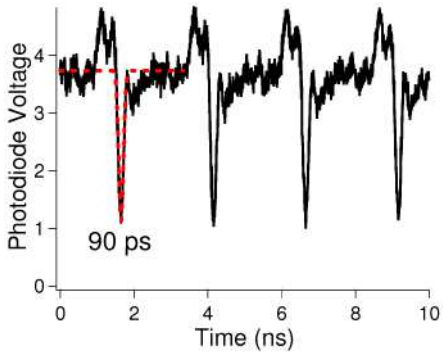


Fig. 4. Output train of dark pulses detected by a photodiode. Red dashed line shows fit to a single pulse for pulsewidth determination .

The stability of the pulse train was confirmed by the clear comb with narrow lines in the radio frequency spectrum of the photodiode output (shown in Fig. 5). The peak at 400 MHz

#127499 - $15.00 USD Received 23 Apr 2010; revised 22 May 2010; accepted 25 May 2010; published 7 Jun 2010

matches the cavity-round trip time and tracks exactly any length changes of the extended cavity.

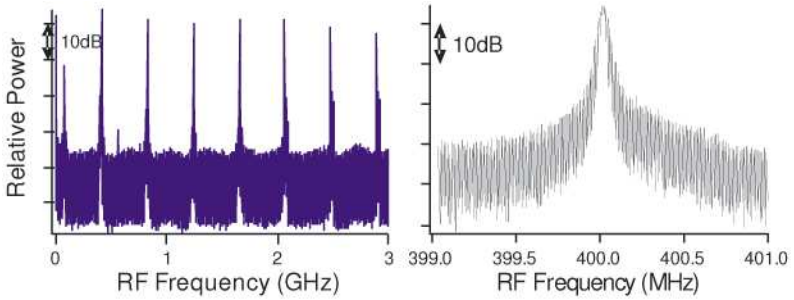


Fig. 5. RF power spectrum of photodiode output at a 110 mA bias current for a wide span (left) and zooming in the on the fundamental (right, resolution bandwidth is 2kHz).

The optical spectrum is centered at 1167 nm, which corresponds to laser emission from the QD ground state, and the bandwidth is about 0.5 nm (0.2 THz) as shown in Fig. 6.

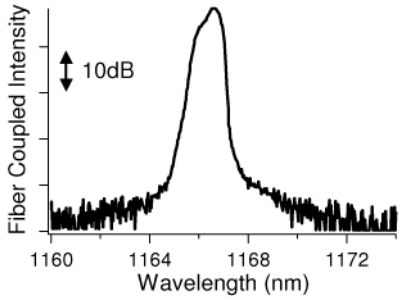


Fig. 6. Optical spectrum at bias current of 110 mA. Bandwidth is about 0.5 nm (resolution bandwidth is 0.07 nm).

We recorded the dark pulse train as a function of lasing wavelength by tuning the laser from 1162 nm to 1178 nm using the intracavity Fabry-Perot etalon. The dark pulse width and modulation depth changed with wavelength as shown in Fig. 7. Over this range, the shortest measured pulse width was 90 ps at 1168 nm (red dots in Fig. 7). The modulation depth varied between 70% and 80% in the lasing range (blue triangles in Fig. 7). The lasing wavelength of 1168 nm is matched with the R-SBR resonant wavelength. As we move away from this wavelength the pulse shaping due to the R-SBR is reduced, resulting in an increase of the dark pulse width.

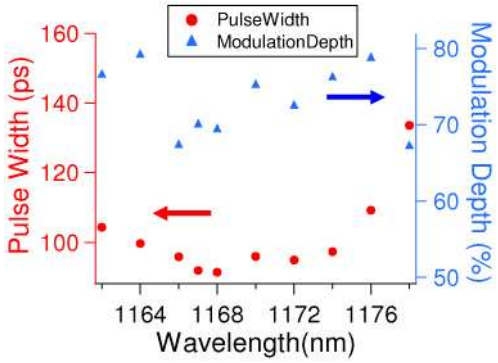


Fig. 7. Dark pulse width and modulation depth variation with lasing wavelength.

#127499 - $15.00 USD Received 23 Apr 2010; revised 22 May 2010; accepted 25 May 2010; published 7 Jun 2010

## 3. Simulations

The theoretical understanding of mode-locked lasers typically starts from the "master equation" model developed by Haus [25]. In steady-state, the pulse must reproduce itself every round-trip. Considering only fast saturable gain, fast saturable absorption and spectral filtering, yields the steady state condition

$$\left[ l_o + \frac{q_0}{1+|u|^2/I_q} - \frac{g_0}{1+|u|^2/I_g}\left(1+\frac{1}{\omega_g^2}\frac{d^2}{dt^2}\right) - \frac{1}{\omega_f^2}\frac{d^2}{dt^2} \right] u = 0 \qquad (1)$$

where $u$ is the pulse amplitude, $q_0$ ($g_0$) is the small-signal absorption (gain) coefficient, $l_0$ is the non-saturable loss in the cavity, $I_a$ ($I_g$) is the saturation power for to absorption (gain), $\omega_g$ is the gain bandwidth and $\omega_f$ is the filter bandwidth. Neglecting nonlinear and dispersion effects is justified by the low peak power and moderate pulse bandwidth. Equation (1) cannot be solved analytically, so we start by linearizing the gain and absorption saturation terms, also with the assumption that $\omega_f$ is smaller than $\omega_g$, giving

$$\left[ l_0 + q_0\left(1-\frac{|u|^2}{I_q}\right) - g_0\left(1-\frac{|u|^2}{I_g}\right) - \frac{1}{\omega_f^2}\frac{d^2}{dt^2} \right] u = 0. \qquad (2)$$

A bright pulse of the form $u = u_0 \operatorname{sech}\left(t/\tau_p\right)$ is a solution to this equation, however it is not self starting [19]. Another solution has the form of $u = u_0 \tanh\left(t/\tau_p\right)$, which is a dark pulse. This solution corresponds to a CW wave of amplitude $u_0$ with a dip at $t = 0$ that has a width $\tau_p$. The CW wave before the dip has $\pi$ phase shift compared to that after the dip. While this analysis shows that a dark pulse is a solution, it does not show that it is stable against perturbations, which is also a requirement for it to exist in a physical system such a laser. Stability arises from the interplay of saturation and spectral filtering. To study stability, we numerically simulate Eq. (1). Specifically we start with an initial condition and evolve it according to

$$T_R \frac{\partial}{\partial T} u(T,t) = \left( g + D_{g.f}\frac{\partial^2}{\partial t^2} - l_0 - \frac{q_0}{1+|u|^2/P_A} \right) u(T,t) \qquad (3)$$

where T is slow time, i.e., corresponding to round trips in the cavity.The operator $D_{gf} = \frac{g}{\omega_g^2} + \frac{1}{\omega_f^2}$ describes the finite bandwith of the gain and other spectral filtering effects in the cavity.

In a numerical simulation, additional terms, such as the biexponential gain recovery of QDs, can be added to more accurately model the real laser. We attribute the biexponential decay to intra-dot relaxation and to refilling of the dots from the wetting layer [20,21]. The relaxation times for both of these effects are fast compared to the measured width of the dark pulse, thus the approximation of fast dynamics is valid. The model can better account for this behavior if the fast gain saturation includes two components with differing saturation powers. We include a time dependent gain due to saturation

$$g(t) = \frac{g_n}{1+P/I_g} + \frac{g_l}{1+|u|^2/I_{gl}} + \frac{g_h}{1+|u|^2/I_{gh}} \qquad (4)$$

including two fast gain saturation powers as $I_{gl}$ and $I_{gh}$, and the fast small signal gain also separates into two parts $g_l$ and $g_h$. Furthermore the gain will show very slow saturation determined by the carrier injection rate, which means a slow gain saturation part should be

#127499 - $15.00 USD Received 23 Apr 2010; revised 22 May 2010; accepted 25 May 2010; published 7 Jun 2010

included in the gain simulation model. We define the slow gain saturation power as $I_{gs}$ and the corresponding slow small signal gain $g_n$. We model this effect by including a term that saturates based on the total energy in the cavity, rather than the instantaneous power. A split-step algorithm simulates each round trip through the laser cavity, calculating the saturation terms in the time-domain and the spectral filtering in the frequency domain. Given an arbitrary input condition, usually a pulse, we track the evolution through many round trips until the change between successive round-trips is negligible. To test that the simulation is working properly, we verified that it did produce stable bright pulses with pulse parameters in agreement with previously published results [26].

We find that the simulation produces stable dark pulses when we include the two-component fast gain saturation and the slow gain saturation. The parameters for the simulation are based on our best estimate of the operating conditions of the laser, as described in Section 4 and given in Table 1. Examining how the gain and absorption saturate, as is often done when discussing the stability of bright pulses in a mode-locked laser, gives insight into why the two-component saturation results in stable dark pulses. To provide an intuitive explanation ignoring spectral filtering, we plot the gain and absorption as a function of intensity for (a) single component gain saturation and (b) two-component fast gain saturation in Fig. 8. The net gain is plotted in the lower panel for each case. In both cases, the loss is given by the first two terms in Eq. (1) and the intensity is normalized to $I_q$. Figure 8(a) shows the saturation curves for the situation where the absorber has lower saturation intensity than the gain, but the unsaturated absorption is higher than the unsaturated gain. For this situation, there are two intensities at which the gain and loss cross. To the left of the lower point, denoted by "L" in Fig. 2(a), there is net loss, so intensities in this range will decay to zero. To the right of L, but to the left of the upper crossing point, denoted by "U", there is net gain, so intensities in this range will grow to intensity U. To the right of U, the again there is net loss, so the intensity will decay back to point U. It is easy to see that an initial bright pulse, or fluctuation, that exceeds intensity L will grow until its peak intensity reaches U. This simple picture yields a threshold behavior, which produces a rectangular bright pulse. Including a spectral filter limits the rise and fall times of the pulse, resulting in a smooth pulse with a minimum duration determined by the bandwidth of the spectral filter.

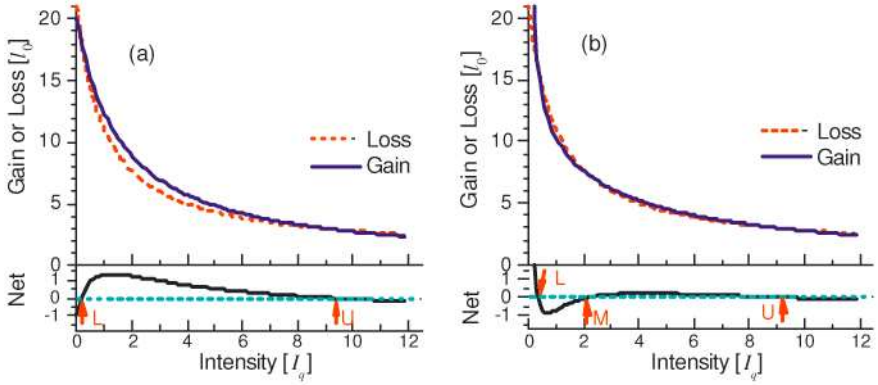


Fig. 8. Saturation of the absorption and (a) single component gain and (b) two component gain. The power is in units of the absorber's saturation power, $I_q$. and the gain and loss are in units of the nonsaturable loss, $l_0$. The lower panel in (a) and (b) show the net gain (gain minus loss). The points where the net gain is zero are stationary and labeled.

By similar reasoning, it initially appears that these conditions would also support a dark pulse. Consider CW operation at power U, which is stable, with a fluctuation that drops below the intensity corresponding to point L. Again the threshold will drive the fluctuation to zero intensity, resulting in a rectangular dark pulse when the spectral filter is omitted. However, in contrast to the bright pulse, simulations show that the inclusion of the spectral filter actually destabilizes the dark pulse, causing it to evolve into a bright pulse.

#127499 - $15.00 USD Received 23 Apr 2010; revised 22 May 2010; accepted 25 May 2010; published 7 Jun 2010

Stable dark pulses appear in the simulation when we include two-component fast gain saturation and slow gain saturation in the model. Figure 8(b) shows the saturation curves for conditions that give a stable dark pulse. A third crossing point, denoted by "M" in Fig. 8(b), occurs with net loss below it and net gain above. CW lasing at an intensity above that corresponding to M will evolve to intensity U. If an intensity fluctuation occurs that crosses to the left M, it will evolve towards L. Again, if the spectral filter is omitted, a rectangular dark (gray) pulse will result. However, the inclusion of the spectral filter results in a stable smooth dark pulse. The evolution of an initial bright pulse into a stable dark (actually gray) pulse is shown in Fig. 9. The evolution is also shown in Fig. 10 as an animation. Since the simulation does not include phase, the solution could be a chirped pulse.

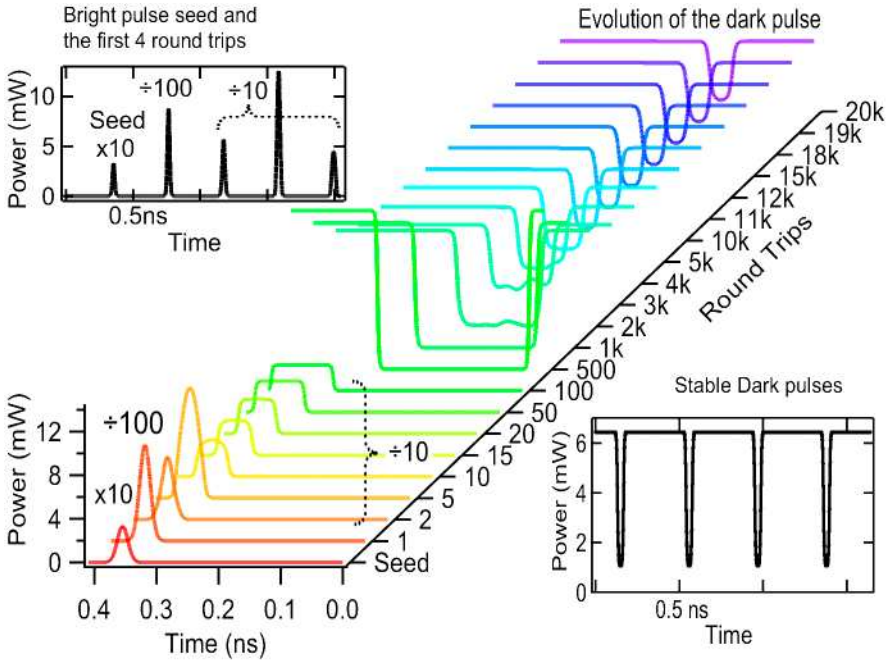


Fig. 9. Evolution of initial bright pulse seed into a steady state solution showing a gray pulse, the stable dark pulse width is 36 ps and the modulation depth is 84%.

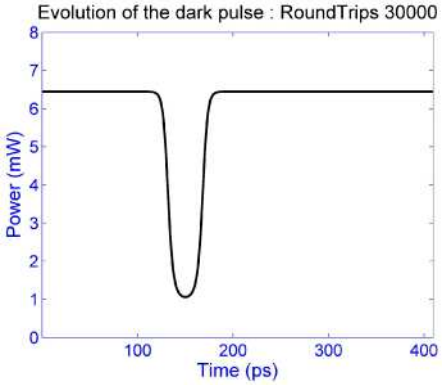


Fig. 10. (Media 1) Animation of the evolution shown in Fig. 9.

We systematically explored parameter space to determine if the formation of dark pulses is a robust phenomenon. For each parameter set, we run the simulation until a steady state evolves. We then categorize the steady state as being (i) CW, defined as having an intensity

#127499 - $15.00 USD Received 23 Apr 2010; revised 22 May 2010; accepted 25 May 2010; published 7 Jun 2010

modulation less than 10%, (ii) a dark pulse, defined as a dip in the intensity of greater than 10% with dark duration that is less than 40% of the round trip time, (iii) a bright pulse, defined as a positive going excursion in the intensity of greater than 10% with bright duration that is less than 40% of the round trip time, or (iv) a pulsation, which is a modulation of greater than 10% that does not fulfill the criteria for a bright or dark pulse. Note that our definition of a dark pulse allows for a gray pulse and the definition of a bright pulse allows it to ride on a CW background. In Fig. 11, we plot "phase space" diagrams for the laser showing what type of output it gives as we vary the two fast gain saturation parameters (high fast gain saturation power $I_{gh}$ and low fast gain saturation power $I_{gl}$, both are normalized to the absorber saturation power $I_q$). As $I_{gh}$ increases, the laser goes from CW to dark pulses to pulsations and finally to bright pulses. This sequence remains the same as $I_{gl}$ is varied, although the transition between the regimes varies as $I_{gl}$ is increased. We have also varied other parameters and find that the basic structure of this map does not change. The shading in the dark pulse region denotes the modulation depth of the stable dark pulses. The darker the region, the closer the modulation is to 100% (black pulse). The dark pulse modulation depth increases (the dark pulses change from gray pulses to black pulses) when $I_{gh}$ or $I_{gl}$ is increased.

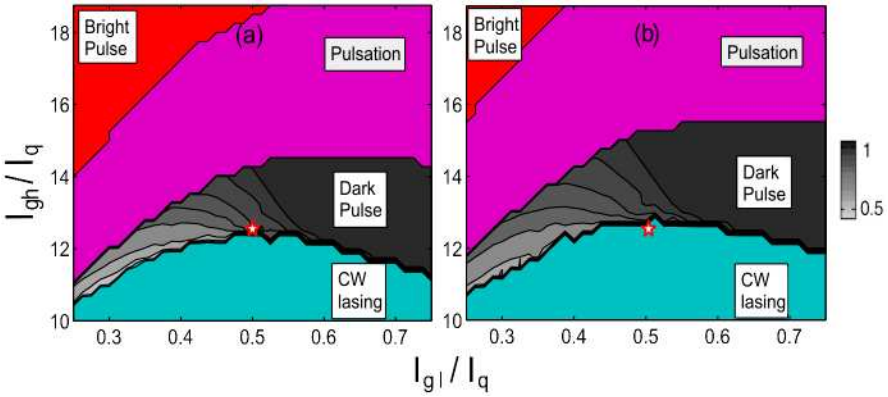


Fig. 11. Phase space maps showing stable solution as a function of low, $I_{gl}$, and high, $I_{gh}$, saturation powers for the gain, normalized to the absorption saturation power, $I_q$. The gray scale bar indicates the modulation depth of the dark pulse. In (a), the star indicates the best estimate of the operating point (parameters listed in Table 1) for the experimental conditions when the laser produces dark pulses. The experimental conditions, an increase of slow gain by 4%, where the laser produces CW output is shown in (b), again the star indicates the estimated operating point.

## 4. Estimation of operating conditions

To compare our experimental results to the simulation, we have made our best estimate of the operating parameters corresponding to the experimental observation of dark pulses.

From the QDs' cross section and gain dynamics, we estimate the saturation power of the QDs gain. The saturation power is $I_{sat} = \frac{\hbar\omega}{\sigma T_1} A$, where $\hbar\omega$ is the photon energy, $T_1$ is the recovery time of the absorber, $\sigma$ is the absorption cross section and $A$ is the mode area. The absorption cross section is $\sigma = \frac{\lambda^2}{2\pi}\frac{\gamma_{rad}}{\omega_g}$ [23]. The spontaneous emission time, $1/\gamma_{rad}$, for a quantum dot is around 500 ps [27], and a single quantum dot's emission bandwidth, $\omega_g$, is around 10 nm with a Lorentzian lineshape, yielding an absorption cross section of approximately $4\text{x}10^{13}$ cm$^2$ at a wavelength, $\lambda$, of 1170 nm. The QD gain has multiple recovery times [20,21]. In Fig. 12, a pump-probe measurement of the QD recovery time in the waveguide under 50 mA current injection is plotted. The two components of the fast recovery have time constants $T_{1h}$ = 100 fs and $T_{1l}$ = 2.5 ps corresponding to fast saturation powers

#127499 - $15.00 USD Received 23 Apr 2010; revised 22 May 2010; accepted 25 May 2010; published 7 Jun 2010

around 100 mW ($I_{gh}$) to 4 mW ($I_{gl}$) for 2 μm$^2$ mode area. The slow recovery time is several hundred picoseconds. The slow gain saturation power, $I_g$, is about 3 mW.

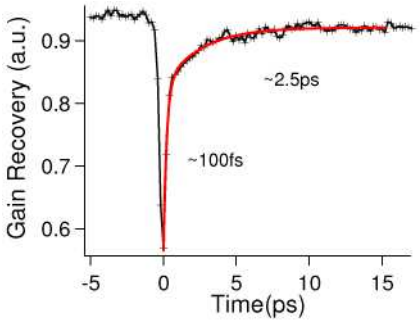


Fig. 12. Pump-probe measurement showing the recovery of the QD amplifier gain.

We measure the total small signal gain ($g_n$ + $g_l$ + $g_h$) to be approximately 12 cm$^{-1}$. Thus for a 5 mm long laser bar, the total normalized gain is 6. However, it is difficult to accurately calculate the small signal gains for different gain saturation powers. We estimate the ratio of the two fast recovery gain parts, $g_l$ and $g_h$, from the double exponential curve fit coefficients in Fig. 12, the coefficient of the ~100 fs part is 5 times bigger than that of the 2.5 ps part. Thus we use this ratio for small signal gain values.

The total cavity loss is high in the diode laser. The output facet reflection, $R_1$, is 35%, and the reflectivity of the Bragg reflector, $R_2$, is 50% (low-intensity) to 70% (saturation), plus the coupling efficiency, $\eta$, is 80%, so the normalized loss term, $\alpha = -\ln(R_1 * R_2 * \eta)$, varies from 1.9 (low-intensity) to 1.6 (saturation). Thus the cavity loss, $l_o$, is 1.6, and the small signal absorber loss ($q_0$) is 0.3.

Based on these estimates, we use the parameters listed in Table 1 in the simulation to model the behavior of the laser.

**Table 1. Parameter estimates for operating conditions of laser**

| Symbol | Parameter Description | Units | Value | source |
|---|---|---|---|---|
| $g_n$ | slow small signal gain | - | 5 | M, E |
| $I_g$ | slow gain saturation power | mW | 3 | C, M, Refs |
| $g_l$ | gain for low fast saturation power | - | 0.15 | M, E |
| $I_{gl}$ | low fast gain saturation power | mW | 4 | C, M, Refs |
| $g_h$ | gain for high fast saturation power | - | 0.75 | M, E |
| $I_{gh}$ | high fast gain saturation power | mW | 100 | C, M, Refs |
| $l_o$ | cavity loss | - | 1.6 | C |
| $q_0$ | absorber small signal loss | - | 0.3 | C |
| $I_q$ | absorber saturation power | mW | 8 | M, C |
| $\omega_g$ | Gain bandwidth | THz | 10 | E |
| $\omega_f$ | filter effect bandwidth (from lens coupling and F-P filter) | THz | 0.7 | E |
| E: Estimated; C: Calculated; M: Measured; Refs [20,21,27]: | | | | |

#127499 - $15.00 USD Received 23 Apr 2010; revised 22 May 2010; accepted 25 May 2010; published 7 Jun 2010

We mark the position corresponding to our best estimates of the lasers operating conditions wit stars in Fig. 11. For experimental conditions that produce dark pulses, corresponding to Fig. 11(a) and the parameter values give in Table 1, the operating conditions fall well with the region where the simulation produces dark pulses, and indeed the modulation depth is similar to what we observe. Experimentally, systematic variation of the operating parameters is difficult. We did increase the injection current and find that a transition from dark pulses to CW operation occurs. A higher injection current means a larger slow gain, $g_n$. In Fig. 11(b), we show the phase space diagram for a larger slow gain, $g_n = 5.2$, where CW operation occurs and find that our best estimate of the operating point falls within the region predicted for CW operation.

## 5. Summary

Our results experimentally demonstrate a new operating regime for mode-locked diode lasers, namely the generation of a train of dark pulses. The theoretical analysis shows that dark pulses are solutions to the master equation describing mode-locked lasers and simulations show that dark pulses are stable. The complex dynamics of the QD active region stabilize the dark pulse train. Having net normal dispersion was essential in prior demonstrations of dark pulse generation in mode-locked fiber lasers [18,28], which means that the interplay between nonlinearity and dispersion dominated the pulse shaping. In contrast, the simulations suggest that shaping due to the saturable absorber dominates in our experiments.

#127499 - $15.00 USD Received 23 Apr 2010; revised 22 May 2010; accepted 25 May 2010; published 7 Jun 2010